AIP | Physics of Fluids

Simulations of nonlinear pore-water convection in spherical shells

Zifeng Dai, Keke Zhang, Gerald Schubert, and Xinhao Liao

Citation: Phys. Fluids **20**, 026601 (2008); doi: 10.1063/1.2839052

View online: http://dx.doi.org/10.1063/1.2839052

View Table of Contents: http://pof.aip.org/resource/1/PHFLE6/v20/i2

Published by the American Institute of Physics.

Simulations of nonlinear pore-water convection in spherical shells

Zifeng Dai,[1] Keke Zhang,[1] Gerald Schubert,[2] and Xinhao Liao[3]
[1]*Center for Geophysical and Astrophysical Fluid Dynamics and Department of Mathematical Sciences, University of Exeter, Exeter EX4 4QE, United Kingdom*
[2]*Department of Earth and Space Sciences and Institute of Geophysics and Planetary Physics, University of California, Los Angeles, California 90095-1567, USA*
[3]*Shanghai Astronomical Observatory, Chinese Academy of Sciences, Shanghai 200030, China*

(Received 9 November 2006; accepted 17 December 2007; published online 14 February 2008)

Hydrothermal convection of pore water of uniform viscosity within a permeable, internally heated spherical shell bounded by two concentric spherical surfaces of inner radius r_i and outer radius r_o is investigated by fully three-dimensional numerical simulations based on a domain decomposition method. We first determine the critical Rayleigh number for the onset of hydrothermal convection by expressing linear solutions in terms of spherical Bessel functions. It is found that the basic motionless state becomes unstable with respect to an infinitesimal disturbance characterized by a spherical harmonic of degree l, the size of which is strongly dependent upon the aspect ratio r_i/r_o. However, the three-dimensional structure of convection cannot be determined by the stability analysis because of the mathematical degeneracy of the linear solution. A new numerical scheme using a finite difference method is then employed to simulate three-dimensional nonlinear convection near the onset of convection. When the aspect ratio $(r_o-r_i)/r_o$ is moderately small, a large number of different stable stationary patterns with exactly the same Rayleigh number are found by using different initial conditions. The solutions are relevant to the convectively forced circulation of water in the interiors of early solar system bodies and outer planet icy satellites.
 [DOI: 10.1063/1.2839052]

I. INTRODUCTION

Carbonaceous chondrite (CC) meteorites preserve a record of conditions in the early history of our solar system. The record endures in the elemental and isotopic composition and mineralogy of these primitive objects. Among the minerals found in CCs are ones such as phyllosilicates that form as products of the low temperature interaction of rocks with liquid water. In order to interpret the mineralogic and isotopic data from CCs, it is necessary to understand the nature of the hydrothermal reactions that took place in the early solar system parent bodies of these meteorites. The parent bodies from which the CCs derive were undoubtedly tens to hundreds of kilometers across and originally consisted of ice and rock. The heat of decay of short-lived radioactive elements such as ^{26}Al melted the ice in the CC parent bodies and created the environment in which water-rock interactions altered the mineral content of these bodies. As shown by Grimm and McSween[1] and Young *et al.*,[2] it is likely that liquid water did not simply fill the porosity of the parent bodies but circulated in a convective manner similar to what is observed in geothermal systems in Earth's crust. It is important to understand the nature of this hydrothermal circulation in order to predict the mineralogic composition of the parent bodies at the conclusion of the process. The CCs are relic samples of the final stages of the parent body alteration.

Motivated by understanding the physical conditions required to excite pore water convection in carbonaceous chondrite parent bodies, Young *et al.*[2] calculated the critical Rayleigh number for the onset of pore water convection within the pore space of a permeable sphere. The three-dimensional structure of the convective flow in full spheres was then determined by removing the degeneracy through the nonlinear effect on the basis of a perturbation analysis (Zhang *et al.*[3]). Porous medium convection in spheres represents a particularly simple mathematical problem because the linear solution is characterized by the spherical harmonics $Y_l^m(\theta,\phi)$ of degree $l=2$, representing the only case in which the degeneracy can be completely removed by the solvability condition in the weakly nonlinear perturbation analysis.

Though the critical Rayleigh number for a spherical shell can be determined analytically, the structure of the convective flow cannot be so determined because of the well-known degeneracy of the linear problem in spherical geometry (for example, Young;[4] Busse[5]). In a spherical shell with inner radius r_i and outer radius r_o, the problem of hydrothermal convection becomes much more complicated since the critical eigenfunction usually corresponds to the spherical harmonics $Y_l^m(\theta,\phi)$ of degree $l \gg 1$. When the aspect ratio r_i/r_o is moderate, the selection of the nonlinear patterns bifurcating from a spherically symmetric basic state poses a complicated and difficult problem. At the onset of spherical hydrothermal convection, i.e., $\mathrm{Ra}=\mathrm{Ra}_c$, where Ra is the Rayleigh number, and the general linear solution may be written, for example, as

$$u_r = f_l(r)\sum_{m=0}^{m=l}(C_m\cos m\phi + S_m \sin m\phi)P_l^m(\cos\theta), \qquad (1)$$

where (r,θ,ϕ) are spherical polar coordinates, u_r is the radial flow, $f_l(r)$ represents a radial eigenfunction, $P_l^m(\cos\theta)$

denotes standard spherical harmonics of degree l and C_0, C_m, S_m, $m=1,\ldots,l$ are $(2l+1)$ arbitrary constants. The value of l corresponds to the minimum Rayleigh number Ra_c required to initiate convection. Equation (1) indicates that there exists a $(2l+1)$-fold degeneracy of the solution. A complete elimination of the $(2l+1)$-fold degeneracy by nonlinearity proves to be a mathematically challenging task. Busse[5] used the solvability conditions for the weakly nonlinear problem to select the nonlinear pattern of the flow for small values of l with an assumption that all solutions of the nonlinear problem possess symmetry with respect to a plane through the center of the sphere to simplify the mathematical analysis. By taking the plane at $\phi=0$, the assumption of symmetry with respect to the plane leads to

$$S_m = 0, \quad m = 1, \ldots, l, \tag{2}$$

in Eq. (1). Consequently, the $(2l+1)$-fold degeneracy of the solution is reduced to an $(l+1)$-fold degeneracy. Matthews[6] employed the group theoretical method (see also Chossat[7]) to classify the nonlinear solutions that may exist in the vicinity of the bifurcation point. Both the approaches are based on the second-order expansion near the threshold for an abstract mathematical system in a spherical shell.

The degeneracy arising from the current hydrothermal convection represents a much more complicated problem, because the mathematical equations and the relevant boundary conditions governing hydrothermal convection are self-adjoint. Consequently, the usual weakly nonlinear theory (e.g., Busse;[5] Matthews[6]) based on the second-order expansion cannot be used. There exist no mathematical theories that can predict, in the vicinity of instabilities, if there exist any stable nonlinear solutions or how many stable solutions are possible at a given l and whether the stable solutions are oscillatory or stationary. In this case, it becomes necessary to use a fully numerical analysis to determine the three-dimensional structure of the convective flow in a spherical shell porous medium even for weakly nonlinear solutions. This work presents both the linear stability analysis determining both the critical Rayleigh number Ra_c and the corresponding critical degree l_c for the onset of hydrothermal convection, which is necessary for understanding the weakly nonlinear problem, and the fully three-dimensional numerical simulations revealing a variety of nonlinear convection patterns near the onset of convection. Apart from planetary applications, the problem of nonlinear hydrothermal convection in a spherical shell also provides an ideal physical system for understanding the unsolved problem of nonlinear pattern selection with a large degree of mathematical degeneracy in spherical geometry.

It is important to note that the mathematical equations governing porous medium convection are fundamentally different from ordinary thermal convection, which has been extensively studied (for example, Schubert;[8] Schubert and Zebib;[9] Glatzmaier;[10] Zhang and Busse;[11] Zhong *et al.*;[12] Yuen *et al.*;[13] Stemmer *et al.*;[14] and Chan *et al.*[15]). The equation of motion for porous medium convection is described by Darcy's law. The applicability of Darcy's law to the problem of hydrothermal convection in CC parent bodies depends on the magnitude and length scale of the porosity. By assuming the validity of porous medium convection governed by Darcy's law, we hypothesize that CC parent bodies have porosities of at most several tens of percent with pore dimensions that are small compared with the size of the parent body. Darcy's law associates a permeability with a rocky assemblage. Even unlithified material like the lunar regolith has a relatively small permeability (10^{-11} m^2) that might be a representative upper bound to the permeability of CC parent bodies (Young *et al.*[2]).

Porous medium convection also differs from ordinary convection in that the velocity boundary condition at the bounding surfaces of the spherical shell requires only the vanishing of the radial flow. This unique feature—Darcy's law and simple boundary conditions—suggests a new numerical method for three-dimensional simulations in spherical-shell geometry. The method makes use of a poloidal-toroidal decomposition in the representation of divergence-free convective flows without having to deal with the higher-order finite difference in the numerical analysis. By adopting an implicit scheme in the radial direction and an explicit scheme in the azimuthal and latitudinal directions, we make effective use of the domain decomposition method by dividing a spherical shell into subdomains in the form of watermelon cuts, leading to efficient three-dimensional simulations on modern parallel computers.

In what follows, we first present the model and mathematical formulation in Sec. II. The linear stability analysis is discussed in Sec. III. Section IV presents the method and results of three-dimensional simulations for nonlinear convection, Sec. V discusses the planetary relevance of the nonlinear solutions, and Sec. VI concludes with a summary and some remarks.

II. MODEL AND MATHEMATICAL FORMULATION

We consider water-saturated permeable porous material confined in a spherical shell with inner radius r_i and outer radius r_o. The whole spherical domain $0 < r^* \leq r_o$, where r^* is the distance from the center of the sphere, is heated by a uniformly distributed internal heat source that produces an unstable radial temperature gradient

$$\partial T_0^*/\partial r^* = -\beta r^*,$$

where T_0^* is the conduction temperature, $\mathbf{r}^*$ is the position vector, and β is a positive constant. Water fills all of the pore space in the shell with volumetric porosity Φ. When β is sufficiently small, we expect a purely conducting state without convection described by

$$\mathbf{g} = -\gamma \mathbf{r}^* = -\left(\tfrac{4}{3}\pi\rho_b G\right)\mathbf{r}^*, \tag{3}$$

$$T_0^* = T_c^* - \tfrac{1}{2}\beta(r^*)^2, \tag{4}$$

$$\nabla P_0^* = -(\gamma\rho_0)\mathbf{r}^*, \tag{5}$$

where $\mathbf{g}$ is the acceleration of gravity, T_c^* is the temperature at the center of the sphere, P_0 is the pressure, G is the gravitational constant, and ρ_b is the bulk density

$$\rho_b = (1-\Phi)\rho_r + \Phi\rho_w. \tag{6}$$

Here, ρ_r and ρ_w are the densities of rock and water, respectively. We use spherical polar coordinates (r^*, θ^*, ϕ^*) with $(\hat{\mathbf{r}}, \hat{\boldsymbol{\theta}}, \hat{\boldsymbol{\phi}})$ the corresponding unit vectors.

For a given size of the spherical shell, r_i, and r_o, hydrothermal convection can take place if the unstable temperature gradient β is sufficiently large. We use $\mathbf{u}^*$ to represent the Darcy velocity of convection, the volumetric flow rate of water per unit area of the porous medium. In the problem of pore water convection, the Darcy velocity $\mathbf{u}^*$, and the departures of temperature and pressure from their values in the basic state, denoted by Θ^* and P^*, respectively, are governed by Darcy's law, the equation of continuity, and the heat equation

$$0 = -\nabla P^* + \rho_w \alpha \gamma \mathbf{r}^* \Theta^* - \frac{\mu}{k}\mathbf{u}^*, \tag{7}$$

$$0 = \nabla \cdot \mathbf{u}^*, \tag{8}$$

$$c_b \frac{\partial \Theta^*}{\partial t^*} + \rho_w c_w \mathbf{u}^* \cdot \nabla \Theta^* = \beta \rho_w c_w \mathbf{r}^* \cdot \mathbf{u}^* + \sigma_b \nabla^2 \Theta^*, \tag{9}$$

where α is the thermal expansivity of water, c_b is the average heat capacity per unit volume of the water and rock, μ is the viscosity of water, which is assumed to be constant, k is the permeability of the sphere (assumed constant), c_w is the specific heat of water, and σ_b is the average thermal conductivity of the water and rock. The Boussinesq approximation has been made and the condition required for Darcy's law to be valid is that the scale of the porosity is small compared with the radius of the sphere. We assume impermeable and isothermal conditions at the bounding surfaces of the shell; i.e.,

$$\mathbf{r}^* \cdot \mathbf{u}^* = 0, \quad \Theta^* = 0, \quad \text{at } r^* = r_i \quad \text{and } r_o. \tag{10}$$

In deriving the nondimensional equations, we employ the following scales:

$$\mathbf{r}^* = (r_o - r_i)\mathbf{r}, \quad t^* = \frac{(r_o - r_i)^2 c_b}{\sigma_b} t, \quad \mathbf{u}^* = \frac{\sigma_b}{\rho_w c_w (r_o - r_i)}\mathbf{u},$$

$$P^* = \frac{\mu \sigma_b}{k \rho_w c_w} P, \quad \Theta^* = \beta (r_o - r_i)^2 \Theta$$

for length, time, velocity, pressure, and temperature, respectively, which lead to the dimensionless equations

$$0 = -\nabla P + \mathrm{Ra}\mathbf{r}\Theta - \mathbf{u}, \tag{11}$$

$$0 = \nabla \cdot \mathbf{u}, \tag{12}$$

$$\frac{\partial \Theta}{\partial t} + \mathbf{u} \cdot \nabla \Theta = \mathbf{r} \cdot \mathbf{u} + \nabla^2 \Theta, \tag{13}$$

where Ra is the Rayleigh number defined as

$$\mathrm{Ra} = \frac{\alpha \beta \gamma (r_o - r_i)^4}{K\kappa} \tag{14}$$

with $K = \mu/(\rho_w k)$ and $\kappa = \sigma_b/(\rho_w c_w)$. Equations (11)–(13) are subject to the boundary conditions

$$\mathbf{r} \cdot \mathbf{u} = 0, \quad \Theta = 0 \quad \text{at } r = \eta/(1-\eta) \quad \text{and } 1/(1-\eta), \tag{15}$$

where $\eta = r_i/r_o$, the aspect ratio of a spherical shell, is an important parameter of the problem.

Our analysis consists of two major parts. The first is concerned with the linear stability which determines the critical Rayleigh number for the onset of hydrothermal convection. The result of the stability analysis not only provides an essential guide for fully nonlinear simulations, it also helps to understand the results of the nonlinear simulations. The second part involves direct three-dimensional numerical simulations of the nonlinear convection aimed at determining the structure of convection.

III. LINEAR STABILITY ANALYSIS

In the linear stability analysis, we express the Darcy velocity $\mathbf{u}$ in terms of poloidal v and toroidal w components

$$\mathbf{u} = \nabla \times \nabla \times (\mathbf{r}v) + \nabla \times (\mathbf{r}w), \tag{16}$$

which satisfies Eq. (12) automatically. The scalar equations for v and w can be obtained by substituting Eq. (16) into Eq. (11) and then applying the operators $\mathbf{r}\cdot\nabla\times$ and $\mathbf{r}\cdot\nabla\times\nabla\times$ onto the resulting equation, which yields the two equations

$$\mathbf{r} \cdot \nabla \times [\nabla \times (\mathbf{r}w) + \nabla \times \nabla \times (\mathbf{r}v)] = 0, \tag{17}$$

$$\mathrm{Ra}\, L^2 \Theta - \mathbf{r} \cdot \nabla \times \nabla \times [\nabla \times (\mathbf{r}w) + \nabla \times \nabla \times (\mathbf{r}v)] = 0, \tag{18}$$

where L^2 is the differential operator representing the negative Laplacian on a unit sphere

$$L^2 = r^2 \left(\frac{\partial^2}{\partial r^2} + \frac{2}{r}\frac{\partial}{\partial r} - \nabla^2 \right). \tag{19}$$

The linearized heat equation (13) in terms of the poloidal flow v becomes

$$\frac{\partial \Theta}{\partial t} = L^2 v + \nabla^2 \Theta. \tag{20}$$

The boundary condition (15) becomes

$$v = 0, \quad \Theta = 0, \quad \text{at } r = \eta/(1-\eta) \quad \text{and } 1/(1-\eta). \tag{21}$$

After carrying out the vector analysis on Eqs. (17) and (18), we obtain the following linear equations describing the onset of convection

$$L^2 w = 0, \tag{22}$$

$$\mathrm{Ra}\, L^2 \Theta + L^2 \nabla^2 v = 0, \tag{23}$$

$$\frac{\partial \Theta}{\partial t} = L^2 v + \nabla^2 \Theta, \tag{24}$$

Equation (22) implies that the toroidal flow vanishes everywhere. Moreover, it can be readily shown that the linear system (23) and (24) with the boundary conditions (21) is self-adjoint and that exchange of instability is valid; i.e., $\partial\Theta/\partial t = 0$.

At the onset of spherical convection, the general linear solution may be written in the form

$$v = \sum_{m=0}^{m=l} f_l(r)(C_m \cos m\phi + S_m \sin m\phi)P_l^m(\cos\theta), \quad (25)$$

$$\Theta = \sum_{m=0}^{m=l} g_l(r)(C_m \cos m\phi + S_m \sin m\phi)P_l^m(\cos\theta), \quad (26)$$

where $f_l(r)$ and $g_l(r)$ represent the radial eigenfunctions and $P_l^m(\cos\theta)$ is the associated Legendre function of degree l normalized such that

$$\frac{1}{4\pi}\int_0^{2\pi} d\phi \int_0^{\pi} \sin\theta d\theta \{[P_l^m(\cos\theta)e^{im\phi}] \times [P_l^m(\cos\theta)e^{im\phi}]^*\} = 1. \quad (27)$$

Here, the asterisk denotes the complex conjugate. The $(2l+1)$ coefficients C_m, $m=0,1,2,\ldots,l$, and S_m, $m=1,2,3,\ldots,l$ are undetermined. Substitution of Eqs. (25) and (26) into Eqs. (23) and (24) yields

$$\mathrm{Ra}\, l(l+1)g_l(r) - \left[\left(\frac{d^2}{dr^2} + \frac{2}{r}\frac{d}{dr}\right) - \frac{l(l+1)}{r^2}\right]^2 g_l(r) = 0, \quad (28)$$

$$f_l(r) = \left[\frac{\mathrm{Ra}}{l(l+1)}\right]^{1/2} g_l(r). \quad (29)$$

In other words, the general linear solution can be cast in the form

$$\Theta = \sum_{m=0}^{m=l} \{j_l[(\mathrm{Ra}(l+1)l)^{1/4}r] + Q_l n_l[(\mathrm{Ra}(l+1)l)^{1/4}r]\} \times (C_m \cos m\phi + S_m \sin m\phi)P_l^m(\cos\theta), \quad (30)$$

$$v = \sum_{m=0}^{m=l} \left(\frac{\mathrm{Ra}}{l(l+1)}\right)^{1/2} \{j_l[(\mathrm{Ra}(l+1)l)^{1/4}r] + Q_l n_l[(\mathrm{Ra}(l+1)l)^{1/4}r]\} \times (C_m \cos m\phi + S_m \sin m\phi)P_l^m(\cos\theta), \quad (31)$$

where j_l and n_l are spherical Bessel functions of the first and second kind and

$$Q_l = -j_l\left[\frac{(\mathrm{Ra}(l+1)l)^{1/4}\eta}{(1+\eta)}\right] \Big/ n_l\left[\frac{(\mathrm{Ra}(l+1)l)^{1/4}\eta}{(1+\eta)}\right]. \quad (32)$$

The Rayleigh number Ra at the onset of convection is a solution of the equation

$$j_l\left[\frac{(\mathrm{Ra}(l+1)l)^{1/4}\eta}{(1+\eta)}\right] n_l\left[\frac{(\mathrm{Ra}(l+1)l)^{1/4}}{(1+\eta)}\right] - j_l\left[\frac{(\mathrm{Ra}(l+1)l)^{1/4}}{(1+\eta)}\right] n_l\left[\frac{(\mathrm{Ra}(l+1)l)^{1/4}\eta}{(1+\eta)}\right] = 0. \quad (33)$$

For a given η, Eq. (33) can be solved to determine the values of Ra as a function of l. The lowest value of Ra required to excite convection, which is referred to as the critical Rayleigh number Ra_c, is physically relevant.

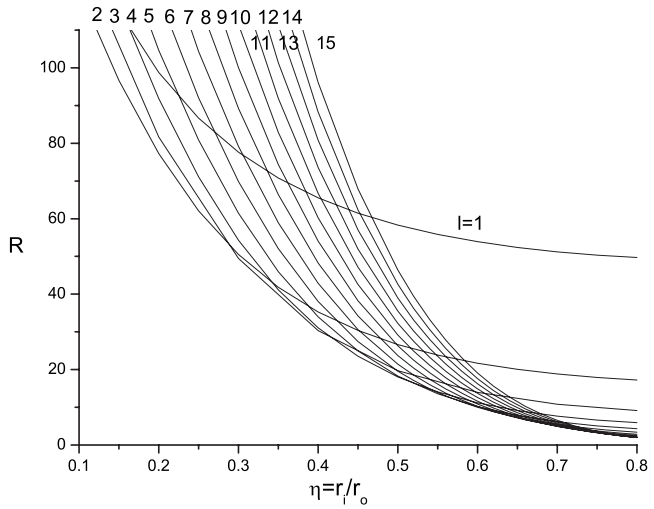

FIG. 1. The marginal Raleigh number Ra is plotted against the aspect ratio η for different values of l at the onset of hydrothermal convection.

The result of the stability analysis is summarized in Fig. 1, showing the marginal Rayleigh number Ra for different l as a function of the aspect ratio $\eta=r_i/r_o$. The $l=1$ mode, the only case in which the structure of the convective flow can be determined uniquely by the stability analysis, is never physically preferred. Note that, in the case of ordinary convection, the critical degree of a spherical harmonic is $l=1$ when the inner core is sufficiently small (Chandrasekhar[16]). For a moderately thick spherical shell with $\eta=0.5$, the critical Rayleigh number Ra_c is located at the degree $l_c=4$, giving rise to a ninefold degeneracy of the linear solution. The critical degree increases to $l_c=14$ corresponding to a 29-fold degeneracy for a thin spherical shell at $\eta=0.8$. In this case, a large number of linear convection modes are clustered near the onset of instabilities, making any mathematical analysis of the weakly nonlinear problem highly formidable. Several typical critical Rayleigh numbers Ra_c and their neighboring values are given in Table I for different aspect ratios of the spherical shell.

TABLE I. Typical values of the marginal Rayleigh number Ra as a function of l for various values of η. The most unstable mode is denoted by the bold number.

l	(η=0.2, Ra)	(η=0.4, Ra)	(η=0.5, Ra)	(η=0.8, Ra)
1	98.9	65.5	58.3	
2	**77.2**	35.3	26.6	
3	81.6	**30.3**	19.7	
4		31.0	**18.0**	
5			18.3	
10				2.134
11				2.040
12				1.985
13				1.959
14				**1.956**
15				1.971

In summary, $(2l+1)$ coefficients, C_m, $m=0,1,\ldots,l$, and S_m, $m=1,\ldots,l$, in the general solution (30) and (31) cannot be determined, resulting in the $(2l+1)$-fold degeneracy of the linear solution. While the critical degree l_c and the radial structure of the flow, $g_l(r)$ and $f_l(r)$, are determined by the linear analysis, the structure of the convective flow remains undetermined when $l_c>1$. When $l_c \gg 1$, a complete or partial elimination of the $(2l+1)$-fold degeneracy by the effect of nonlinearity remains a mathematically challenging task. In the next section, we attempt to determine the structure of three-dimensional convection of pore water in spherical shells via direct numerical simulations.

IV. NONLINEAR CONVECTION

A. The equations for numerical simulation

In order to use the domain decomposition method based on a finite difference scheme, we derive a set of second-order scalar equations from Eqs. (11)–(13) by using expression (16). In a manner similar to deriving the linear equations, we obtain the following three scalar equations governing fully nonlinear convection:

$$\mathrm{Ra}\, L^2\Theta + \nabla^2\Psi = 0, \tag{34}$$

$$L^2 v = \Psi, \tag{35}$$

$$\frac{\partial\Theta}{\partial t} - \Psi - \nabla^2\Theta = -\frac{\Psi}{r}\frac{\partial\Theta}{\partial r} - \frac{1}{r^2}\frac{\partial}{\partial\theta}\left[\frac{\partial(rv)}{\partial r}\right]\frac{\partial\Theta}{\partial\theta} - \frac{1}{(r\sin\theta)^2}\frac{\partial}{\partial\phi}\left[\frac{\partial(rv)}{\partial r}\right]\frac{\partial\Theta}{\partial\phi}, \tag{36}$$

subject to the boundary conditions

$$v = \Psi = \Theta = 0, \tag{37}$$

at the two bounding surfaces $r_i=\eta/(1-\eta)$ and $r_o=1/(1-\eta)$. By introducing a new variable Ψ, the highest order of derivative in the system is the second, permitting a straightforward implementation of finite difference schemes in spherical-shell geometry.

B. The numerical scheme

Our finite difference scheme is based on uniform grids in the azimuthal direction but nonuniform grids in the latitudinal and radial directions. Nonuniform grids are introduced mainly because of the axial singularity in spherical polar coordinates. We examine the heat equation (36) in detail.

Let $(r_k,\theta_j,\phi_l,\ k=1,\ldots,n_r;\ j=1,\ldots,n_\theta;\ l=1,\ldots,n_\phi)$ denote the grid points in spherical polar coordinates and

$$U_k = \frac{1}{2}(dr_k + dr_{k+1}), \quad V_j = \frac{1}{2}(d\theta_j + d\theta_{j+1}),$$

$$W_l = \frac{1}{2}(d\phi_l + d\phi_{l+1}),$$

$$\sin\theta_{j+1/2} = \sin\frac{\theta_j+\theta_{j+1}}{2}, \quad \sin\theta_{j-1/2} = \sin\frac{\theta_j-\theta_{j-1}}{2}.$$

It follows that, for example, the differential operator $\nabla^2\Theta$ at the grid (r_k,θ_j,ϕ_l) can be cast in the difference form

$$\begin{aligned}\frac{1}{2}\nabla^2\Theta_{kjl} = {}& \frac{r_k+U_{k-1}}{r_kU_k(U_k+U_{k-1})}\Theta_{(k+1)jl} + \frac{r_k-U_k}{r_kU_{k-1}(U_k+U_{k-1})}\Theta_{(k-1)jl} + \frac{1}{r_k^2\sin^2\theta_jW_l(W_l+W_{l-1})}\Theta_{kj(l+1)} \\ & + \frac{1}{r_k^2\sin^2\theta_jW_{l-1}(W_l+W_{l-1})}\Theta_{kj(l-1)} + \frac{\sin\theta_{j+1/2}}{r_k^2\sin\theta_jV_j(V_j+V_{j-1})}\Theta_{k(j+1)l} + \frac{\sin\theta_{j-1/2}}{r_k^2\sin\theta_jV_{j-1}(V_j+V_{j-1})}\Theta_{k(j-1)l} \\ & - \frac{r_k(U_k+U_{k-1})-(U_k^2-U_{k-1}^2)}{r_kU_kU_{k-1}(U_k+U_{k-1})}\Theta_{kjl} - \frac{1}{r_k^2\sin^2\theta_jW_lW_{l-1}}\Theta_{kjl} - \frac{\sin\theta_{j+1/2}V_{j-1}+\sin\theta_{j-1/2}V_j}{V_jV_{j-1}(V_j+V_{j-1})}\Theta_{kjl}.\end{aligned} \tag{38}$$

A semi-implicit method, implicit in the radial direction but explicit in both the azimuthal and latitudinal directions, has been used. With this semi-implicit scheme, the time discretization for Eq. (36) can be cast in the form

$$\frac{\Theta^{n+1}-\Theta^n}{\Delta t} - \frac{1}{r^2}\frac{\partial}{\partial r}\left[r^2\frac{\partial}{\partial r}(\Theta^{n+1}-\Theta^n)\right] = \nabla^2\Theta^n + f^n, \tag{39}$$

where Θ^{n+1} and Θ^n denote the temperature at the time steps $t=t_{n+1}$ and t_n, respectively, and f^n represents the terms explicitly evaluated at time $t=t_n$ including the nonlinear term.

Making use of Eq. (38), we obtain a finite difference equation for Eq. (36):

$$\begin{aligned}&\mathcal{A}(\Theta^{n+1}_{(k-1)jl}-\Theta^n_{(k-1)jl}) - \mathcal{B}(\Theta^{n+1}_{kjl}-\Theta^n_{kjl}) \\ &\quad + \mathcal{C}(\Theta^{n+1}_{(k+1)jl}-\Theta^n_{(k+1)jl}) = \mathcal{D},\end{aligned} \tag{40}$$

where

$$\mathcal{A} = \frac{2(r_k-U_k)\Delta t}{r_kU_{k-1}(U_k+U_{k-1})},$$

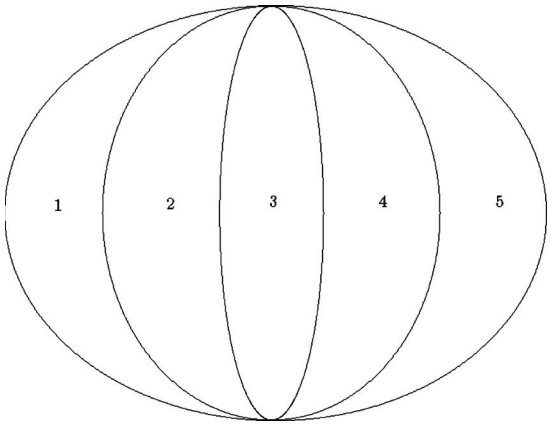

FIG. 2. Sketch of the domain decomposition in spherical-shell geometry.

$$\mathcal{B} = 1 + 2\Delta t\left[\frac{r_k(U_k + U_{k-1}) - (U_k^2 - U_{k-1}^2)}{r_k U_k U_{k-1}(U_k + U_{k-1})} + \frac{1}{r_k^2 \sin^2\theta_j W_l W_{l-1}} + \frac{\sin\theta_{j+1/2} V_{j-1} + \sin\theta_{j-1/2} V_j}{V_j V_{j-1}(V_j + V_{j-1})}\right],$$

$$\mathcal{C} = \frac{2(r_k + U_{k-1})\Delta t}{r_k U_k (U_k + U_{k-1})},$$

$$\mathcal{D} = -\Delta t(\nabla^2 \Theta_{jkl}^n + f_{jkl}^n).$$

An important property of the finite difference equation (40) is that it is tridiagonal and can be therefore readily solved without using an iterative process. Equations (34) and (35) are dealt with in a similar way.

Numerical solutions of the resulting finite difference equations such as Eq. (40) are obtained by dividing the whole spherical shell into N subdomains, where N denotes the number of central processing units available on a parallel computer; they are defined by

$$\frac{2\pi(j-1)}{N} \leqslant \phi \leqslant \frac{2\pi j}{N}, \quad 0 < \theta < \pi,$$

$$r_i \leqslant r \leqslant r_o, \quad j = 1,2,3 \ldots N.$$

The sketch of the domain decomposition is shown in Fig. 2 when $N=5$. At the interface of two subdomains at $\phi_j = 2\pi j/N$, numerical solutions in the neighboring regions are overlapped, leading to the numerical solution for the whole spherical shell. The numerical code is parallelized and highly efficient: the speed of computation for a particular nonlinear convection solution increases typically about 1.7 times when the processor number is doubled.

Before solving the fully nonlinear convection problem, a benchmark comparison is made with an exact solution in order to provide a useful check on the validity and accuracy of the numerical scheme (see the Appendix).

C. The structure of convective flow

The linear stability analysis only determines the critical Rayleigh number Ra_c at which the basic motionless state becomes unstable with respect to infinitesimal disturbances characterized by spherical harmonics of degree l_c. The $(2l_c+1)$-fold degeneracy suggests a multiplicity of convection patterns with exactly the same Rayleigh number. An effective way of obtaining multiple nonlinear solutions is to treat the expected steady nonlinear convection as an initial-value problem, starting numerical integration from carefully chosen different initial conditions. We employ the parametrized initial condition

$$\mathbf{u}(t=0) = \left(\frac{1}{r}L^2\Psi\right)\hat{\mathbf{r}} + \frac{1}{r}\frac{\partial}{\partial\theta}\left[\frac{\partial}{\partial r}(r\Psi)\right]\hat{\boldsymbol{\theta}} + \frac{1}{r\sin\theta}\frac{\partial}{\partial\phi}\left[\frac{\partial}{\partial r}(r\Psi)\right]\hat{\boldsymbol{\phi}}, \tag{41}$$

where Ψ is

$$\Psi = \frac{1}{r}\sin\pi[r - \eta/(1-\eta)]Y_{l_0}^{m_0}(\theta,\phi), \tag{42}$$

l_0 and m_0 being the two parameters of the initial condition.

It is not our purpose to show that, as in any strongly nonlinear system, a final state among the set of nonlinear solutions is highly sensitive to initial conditions. In the present approach, a parametrized initial condition is employed merely as a numerical way of obtaining different convection patterns. In fact, the final state of a nonlinear convection solution describing a weakly nonlinear hydrothermal flow does not sensitively depend upon initial conditions. This is why we have to make a really large perturbation, i.e., change parameters in Eq. (42), in order to reach a different solution numerically.

Consideration in this study is given to three representative cases: a thick spherical shell with aspect ratio $\eta = r_i/r_o = 0.2$, an intermediate thickness shell with $\eta = 0.5$ and a thin shell with $\eta = 0.8$.

We anticipate that the structure of convection in a thick spherical shell at $\eta = r_i/r_o = 0.2$ is largely similar to that in the whole sphere. The analytical study of pore water convection in spheres (Zhang *et al.*[3]) suggests that the only possible structure of nonlinear convection is given by the axisymmetric spherical harmonic $Y_2^0(\theta,\phi)$. The result of our fully three-dimensional simulation is consistent with that prediction. Kinetic energies of the simulated nonlinear convection are displayed in Fig. 3 as a function of time for several Rayleigh numbers and aspect ratio $\eta = 0.2$. All stable nonlinear convection solutions for $\mathrm{Ra}_c = 77.2 < \mathrm{Ra} \leqslant 300$ are found to be stationary. For the weakly nonlinear solution at $\epsilon = (100 - \mathrm{Ra}_c)/\mathrm{Ra}_c = 0.30$, convection is axisymmetric and characterized by the spherical harmonic $Y_2^0(\theta,\phi)$, which is shown in Fig. 4(a). When the Rayleigh number increases to about $\mathrm{Ra} = 150$, a secondary bifurcation takes place and the corresponding convection becomes a mixture of mainly two spherical harmonics $Y_3^2(\theta,\phi)$ and $Y_4^0(\theta,\phi)$. The structure of the nonlinear solution at $\mathrm{Ra} = 300$ is shown in Fig. 4(b). There are no substantial variations in the convection struc-

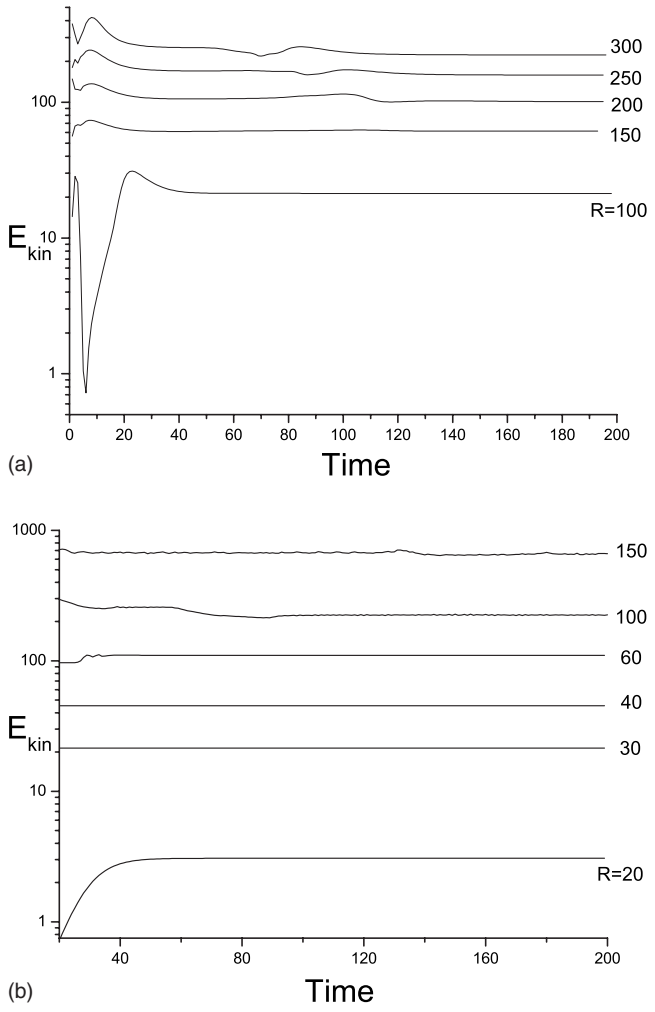

FIG. 3. Kinetic energies of nonlinear convection (a) at the aspect ratio $\eta=r_i/r_o=0.2$ for five different Rayleigh numbers and (b) at the aspect ratio $\eta=r_i/r_o=0.5$ for six different Rayleigh numbers are shown as a function of time.

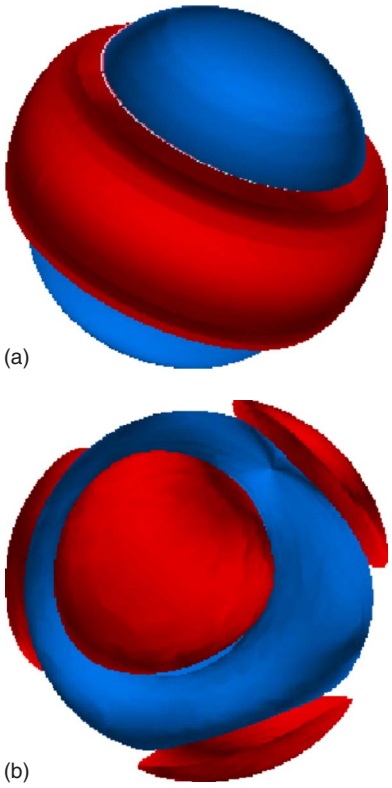

FIG. 4. (Color online) Isosurfaces of the temperature of nonlinear convection at $\eta=r_i/r_o=0.2$: (a) for the Rayleigh number Ra=100 and (b) for Ra =300. Red contours indicate positive temperature $\Theta>0$ and blue contours correspond to negative temperature $\Theta<0$.

ture for Ra in the range $150\leqslant \mathrm{Ra}\leqslant 300$. The thick shell with $\eta=0.2$ represents the simplest case; the convection structure becomes multiform and complicated as the shell becomes thinner.

For a moderately thick spherical shell with aspect ratio $\eta=0.5$, we first consider weakly nonlinear convection at a fixed small Rayleigh number $\epsilon=(\mathrm{Ra}-\mathrm{Ra}_c)/\mathrm{Ra}_c=(20-18.0)/18.0=0.11$. Of course, the heat transport is dependent upon the aspect ratio of the shell, similar to the ordinary convection (Olson and Corcos[17]). For a fixed aspect ratio, the Nusselt number of weakly nonlinear convection is found to be slightly different for different stationary solutions with the same Rayleigh number. For example, the initial condition with $Y_4^0(\phi,\theta)$ leads to the nonlinear solution with the Nusselt number Nu=0.72, while the condition with $Y_4^2(\phi,\theta)$ gives rise to Nu=0.70 (see Fig. 5). This is consistent with nonlinear ordinary convection in various systems (Hansen and Ebel;[18] Stemmer *et al.*[14]).

But different nonlinear solutions may have different total kinetic energies. Our primary aim is to obtain multiple nonlinear convection solutions with the exact same Rayleigh number. The stability analysis shows that the critical convection is characterized by spherical harmonics of degree $l_c=4$; i.e., there exists a ninefold degeneracy in the linear solution. By using different initial conditions, we have found four nonlinear stable patterns of convection with the same Rayleigh number as shown in Fig. 5. All weakly nonlinear solutions in the vicinity of the critical Rayleigh number Ra_c are found to be stationary. It usually takes a few tens of thermal diffusion times for a simulation to reach its stationary state. The azimuthally axisymmetric and equatorially symmetric initial condition with $l_0=4$ and $m_0=0$ in Eq. (41) leads to an axisymmetric stationary convection shown in Fig. 5(a). Its convection pattern on a spherical surface is essentially described by the single spherical harmonic $Y_4^0(\theta,\phi)$, indicating that the stationary bifurcation from the linear solution (30) and (31) with $l=4$, $C_0=1$, $C_m=0$, $m=1,\ldots,4$, and $S_m=0$, $m=1,\ldots,4$ exists and is stable. Moreover, the kinetic energy of the nonlinear convection, i.e., $E_{kin}=3.05$, attains the maximum among different nonlinear solutions with the same Rayleigh number. An initial condition with $l_0=4$ and $m_0=1$ leads to the same pattern apart from a rotational transformation. When the initial condition is azimuthally periodic with $m_0=2$, the final pattern of the convection also becomes azimuthally periodic and dominated by the two spherical harmonics, i.e., $Y_4^2(\theta,\phi)$ and $Y_4^0(\theta,\phi)$, as displayed in Fig. 5(b). By the same procedure, different convection patterns are also obtained from other initial conditions: ($l_0=4$, $m_0=3$) leads to the pattern dominated by the two spherical harmonics, i.e.,

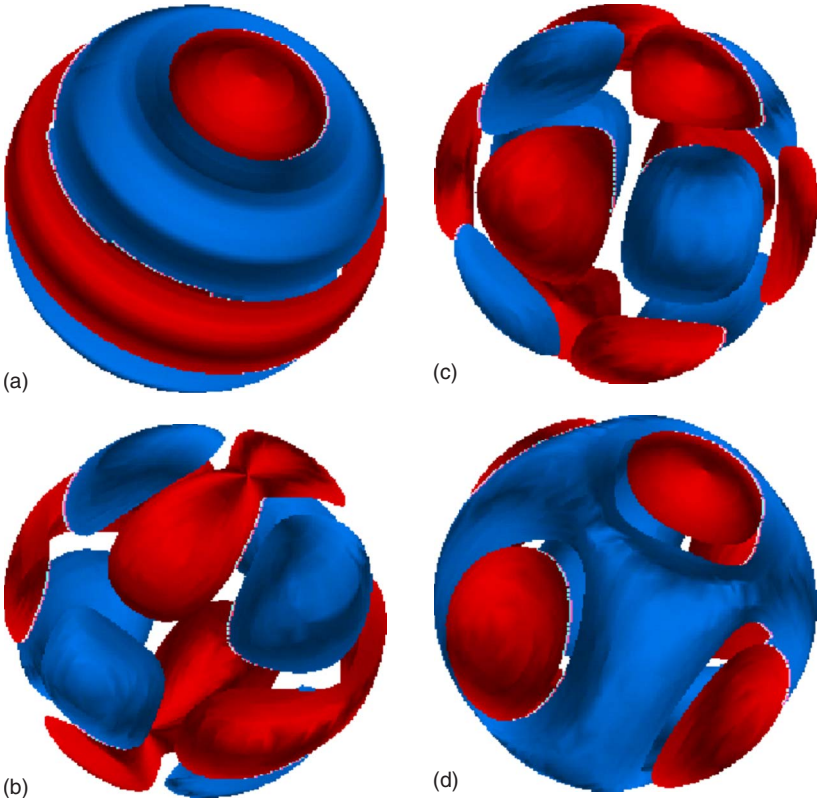

FIG. 5. (Color online) Isosurfaces of the temperature of nonlinear convection at $\eta=r_i/r_o=0.5$ and Ra=20 obtained from four different initial conditions: (a) $Y_4^0(\phi,\theta)$ with $E_{\mathrm{kin}}=3.05$, $Nu=0.723$, (b) $Y_4^2(\phi,\theta)$ with $E_{\mathrm{kin}}=2.28$, Nu=0.698, (c) $Y_4^3(\phi,\theta)$ with $E_{\mathrm{kin}}=2.52$, Nu =0.683, (d) $Y_4^4(\phi,\theta)$ with $E_{\mathrm{kin}}=2.41$, Nu=0.619.

$Y_4^3(\theta,\phi)$ and $Y_4^0(\theta,\phi)$ [Fig. 5(c)], while ($l_0=4$, $m_0=4$) gives rise to the pattern dominated by the two spherical harmonics; i.e., $Y_4^4(\theta,\phi)$ and $Y_4^0(\theta,\phi)$ [Fig. 5(d)]. Our nonlinear simulation suggests that (i) all bifurcations from the linear solution are stationary and (ii) the stationary bifurcation from the linear solution with a single spherical harmonic, i.e., $Y_4^m(\theta,\phi)$, $m>0$, is either nonexistent or unstable. When Ra becomes sufficiently large (Ra$>$200), convection becomes time dependent or chaotic and the complex patterns can no longer be partially elucidated on the basis of the linear stability analysis.

In a thin spherical shell with $\eta=r_i/r_o=0.8$, nonlinear convection becomes extremely complicated because of the existence of a 29-fold degeneracy. It is impossible that all realizable stable solutions near the onset of convection can be found via three-dimensional numerical simulations. Our objective is to reveal that there exist a large number of stable convection patterns with exactly the same Rayleigh number. We restrict our calculations to convection solutions that are equatorially symmetric with respect to the equator plane of a spherical shell, i.e.,

$$(\Theta,u_\theta,u_\phi,u_r)(\theta,\phi,r)=(\Theta,-u_\theta,u_\phi,-u_r)(\pi-\theta,\phi,r);$$

we also confine our calculation to a fixed Rayleigh number $\epsilon=(\mathrm{Ra}-\mathrm{Ra}_c)/\mathrm{Ra}_c=0.11$. Of course, the position of a pole or an equator in our convection system is arbitrary as a consequence of the spherically symmetric basic state and boundary condition. When we refer to an equatorial symmetry or an equator, we always imply that it is in an appropriately chosen spherical coordinate system, which is usually associated with the spatial structure of an initial condition used in our numerical simulations. Eight different nonlinear patterns of convection, shown in Fig. 6, are found by starting numerical simulations with the eight different initial conditions

$$l_0=14,\quad m_0=0,2,4,6,8,10,12,14,$$

at a fixed supercritical Rayleigh number $\epsilon=(\mathrm{Ra}-\mathrm{Ra}_c)/\mathrm{Ra}_c=0.11$, revealing how different initial conditions result in multiple nonlinear patterns near the onset of convection. All the different nonlinear solutions are found to be stationary. In Table II, we summarize the relationship between the initial condition and the dominant spherical harmonics in the stationary convection as well as the kinetic energies of the nonlinear flows. Similar to the case with $\eta=0.5$, the kinetic energy of the axisymmetric nonlinear convection attains the maximum among various nonlinear solutions with the same Rayleigh number. It is remarkable that there exist so many different stable, stationary patterns of hydrothermal convection at exactly the same Rayleigh number, although our numerical approach cannot determine the exact number of stable stationary patterns near the onset of convection. Again, the results of nonlinear simulations suggest that the convection pattern comprises several spherical harmonics near the onset of convective instabilities.

V. PLANETARY RELEVANCE OF THE WEAKLY NONLINEAR SOLUTIONS

In discussing the relevance of the weakly nonlinear solutions obtained here to the problem of hydrothermal convection in the parent bodies of carbonaceous chondrite meteorites, two main issues need to be addressed. One is the spherical shell geometry, and the other is the vigor of convection in the CC parent bodies. Initially, CC parent bodies

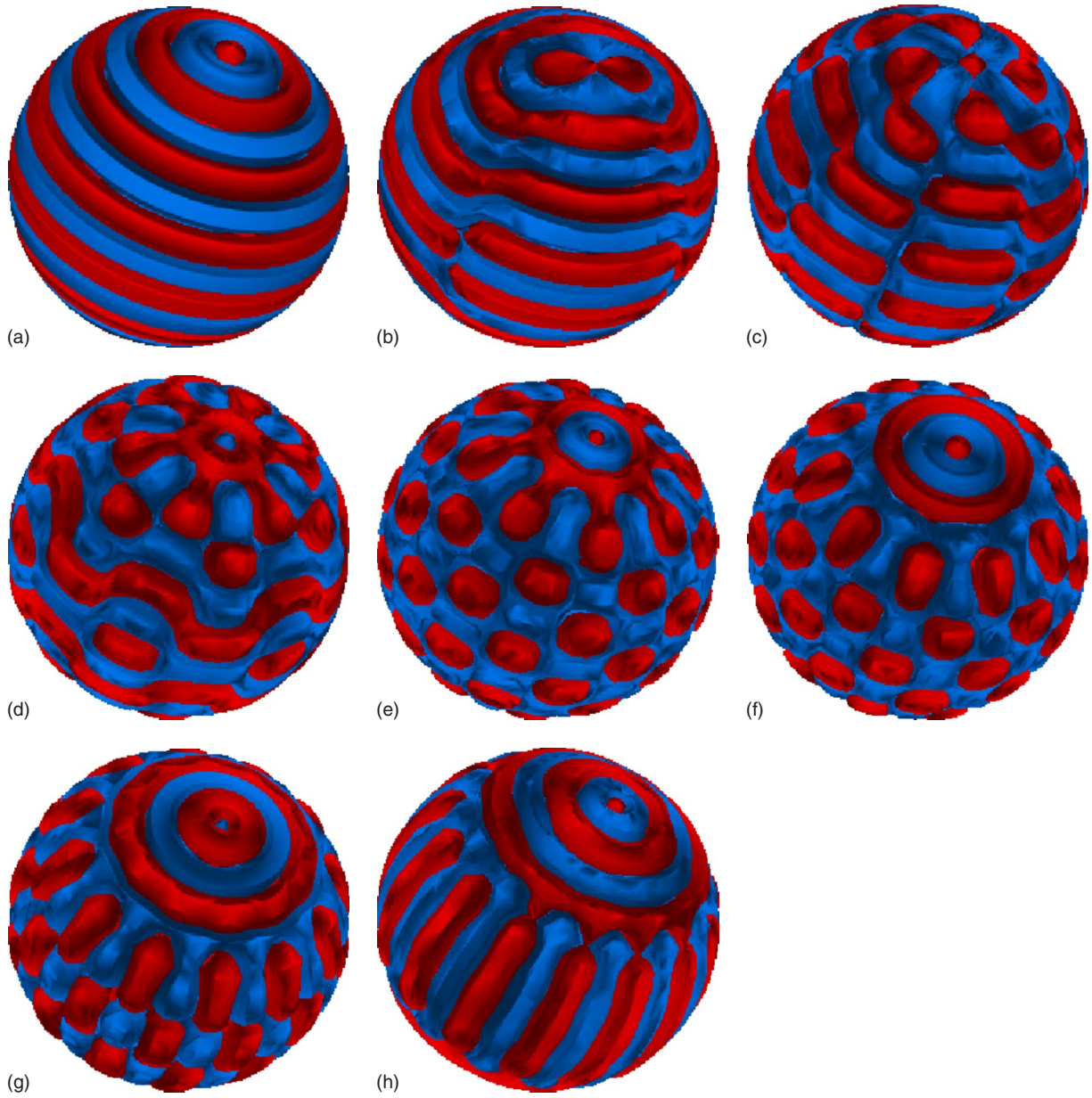

FIG. 6. (Color online) Isosurfaces of Θ of nonlinear convection for $\eta=0.8$ at $\epsilon=(\mathrm{Ra}-\mathrm{Ra}_c)/\mathrm{Ra}c=0.11$, where $\mathrm{Ra}_c=1.956$, obtained with different initial conditions: (a) $Y_{14}^0(\phi,\theta)$, (b) $Y_{14}^2(\phi,\theta)$, (c) $Y_{14}^4(\phi,\theta)$, (d) $Y_{14}^6(\phi,\theta)$, (e) $Y_{14}^8(\phi,\theta)$, (f) $Y_{14}^{10}(\phi,\theta)$, (g) $Y_{14}^{12}(\phi,\theta)$, and (h) $Y_{14}^{14}(\phi,\theta)$.

TABLE II. Dominant spherical harmonics in weakly nonlinear stationary convection solutions at $\epsilon=(\mathrm{Ra}-\mathrm{Ra}_c)/\mathrm{Ra}_c=0.11$ with $\eta=0.8$ obtained by starting simulation from different initial conditions.

Initial condition	Dominant spherical harmonics	Kinetic energies
$Y_{14}^0(\theta,\phi)$:	$Y_{14}^0(\theta,\phi)$, $Y_{16}^0(\theta,\phi)$, $Y_{18}^0(\theta,\phi)$,	0.346
$Y_{14}^2(\theta,\phi)$:	$Y_{14}^2(\theta,\phi)$, $Y_{16}^2(\theta,\phi)$, $Y_{16}^6(\theta,\phi)$,	0.307
$Y_{14}^4(\theta,\phi)$:	$Y_{14}^4(\theta,\phi)$, $Y_{16}^4(\theta,\phi)$, $Y_{14}^0(\theta,\phi)$,	0.290
$Y_{14}^6(\theta,\phi)$:	$Y_{14}^6(\theta,\phi)$, $Y_{14}^0(\theta,\phi)$, $Y_{16}^6(\theta,\phi)$,	0.294
$Y_{14}^8(\theta,\phi)$:	$Y_{14}^8(\theta,\phi)$, $Y_{18}^0(\theta,\phi)$, $Y_{16}^0(\theta,\phi)$,	0.278
$Y_{14}^{10}(\theta,\phi)$:	$Y_{14}^{10}(\theta,\phi)$, $Y_{16}^0(\theta,\phi)$, $Y_{14}^0(\theta,\phi)$,	0.305
$Y_{14}^{12}(\theta,\phi)$:	$Y_{14}^{12}(\theta,\phi)$, $Y_{16}^0(\theta,\phi)$, $Y_{14}^0(\theta,\phi)$,	0.320
$Y_{14}^{14}(\theta,\phi)$:	$Y_{14}^{14}(\theta,\phi)$, $Y_{16}^0(\theta,\phi)$, $Y_{18}^0(\theta,\phi)$,	0.317

were likely intimate mixtures of ice and rock. Short-lived and long-lived radioactivity in the rock heated these bodies, resulting in the melting of the ice. The main question about the CC parent bodies is whether the liquid water was stationary or circulated convectively (Young *et al.*[2]). As a CC parent body was heated, ice at the center would melt first and the heavier rock would sink toward the center and push the water outward. As more ice melted, a liquid water-rock shell would eventually form and the water might undergo hydrothermal convection. The rock matrix would deform and tend to compact toward the center of the body, squeezing the water outward. The time scale for the complete separation of water and rock depends on many poorly known parameters, such as the water/rock ratio, the strength of the rock matrix,

the permeability of the rock matrix, the size of the body, etc. These matters are beyond the scope of this paper. We assume that the consolidation of the rock and the outward migration of the water happens slowly enough that the hydrothermally-induced circulation of water through the spherical shell rock matrix is a phenomenon that occurred in the CC parent bodies. Hydrothermal convection through rocky spherical shells is not only relevant to CC parent bodies, but it is also likely to have occurred or to be presently active in a number of outer planet icy satellites that contain liquid water oceans, among which are Europa and Enceladus (Schubert *et al.*[19]).

With regard to the vigor of convection, it is not expected that hydrothermal convection in CC parent bodies or outer planet icy satellites would be strongly nonlinear. The parameters determining the vigor of convection include the permeability of the rock, the concentration of radiogenic heat sources in the rock, the thickness of the water-rock shell, the viscosity of the water, and other less important parameters. The exact role of all the parameters is given in Eq. (14) for the Rayleigh number, which must exceed a critical value for convection to occur. Values of all these parameters for the CC parent bodies are discussed in Young *et al.*[2] Estimates of the Rayleigh number based on the parameter values in Young *et al.*[2] for a CC parent body about 100 km in radius and with a rock-water shell about 50 km thick result in a value of Ra [from Eq. (14)] less than about ten times the critical value of Ra given in Fig. 1. Therefore, while hydrothermal convection in CC parent bodies of this typical size is expected, the convection is not strongly supercritical, and the weakly nonlinear solutions obtained here should approximate reality.

VI. CONCLUDING REMARKS

This work represents the first study of the multiplicity of convection of pore water of uniform viscosity within a permeable and internally heated spherical shell. The three-dimensional numerical simulations based on a new domain decomposition method reveal the existence of a large number of different stable stationary patterns at exactly the same Rayleigh number in the vicinity of convective instabilities. It provides important insight into a class of important fluid dynamic problems having a large degree of mathematical degeneracy in spherical geometry.

Our theoretical knowledge of the existence and stability of nonlinear solutions of hydrothermal convection in a moderately thin spherical shell is highly limited. We have to tackle the problem by performing fully three-dimensional simulations via different initial conditions while keeping the Rayleigh number unchanged. This numerical approach is of practical utility only and is unrelated to the characteristic feature of a nonlinear system in which a final state of a nonlinear solution is sensitively dependent on initial conditions.

Our approach has the unavoidable consequence that it cannot unveil all the possible stable nonlinear solutions. Nevertheless, on the basis of the numerical simulations, we propose the following conjectures for nonlinear convection near the threshold in moderately thin spherical shells: (i) all weakly nonlinear solutions are stationary and (ii) the stationary nonlinear solution consists of more than one spherical harmonic: the bifurcation from the linear solution of a single spherical harmonic is unstable. The numerical results help to develop a general mathematical theory of nonlinear convection.

It is important to recognize that the problem of hydrothermal convection in spherical shells studied in this paper is self-adjoint. This property imposes difficulties for the ability of the nonlinear theory to remove fully or partially the mathematical degeneracy because the quadratic term in the usual small amplitude expansion is identically zero. Consequently, the higher-order terms play an essential role in determining the structure of nonlinear convection. However, the incorporation of more realistic physics into the model, like the temperature dependence of water viscosity, destroys the self-adjointness of the mathematical problem. In this case, although the analysis becomes more complicated and lengthy, it may permit some theoretical progress towards the understanding of this highly challenging problem.

ACKNOWLEDGMENTS

K.Z. is supported by UK Leverhulme, NERC, and PPARC grants, and G.S. is supported by NASA Planetary Geology and Geophysics Grant No. NNG06GG70G. X.L. is supported by NSFC Grant No. 10633030 and CAS grants. The computation is supported by Shanghai Supercomputer Center (SSC).

APPENDIX: THE VALIDITY OF THE DOMAIN DECOMPOSITION METHOD

In an effort to check the validity, accuracy, and efficiency of the numerical scheme, we first solve the following equation in spherical shells:

$$\frac{\partial H}{\partial t} = \nabla^2 H + f_0(t,r,\theta,\phi), \tag{A1}$$

subject to the boundary condition

$$H(r_i,\theta,\phi) = H(r_o,\theta,\phi) = 0, \tag{A2}$$

where f_0 is a prescribed analytical function. An exact solution for Eq. (A1) is simply given by

$$H_{\text{exact}} = H_0 = \cos(\sin\theta\cos\varphi + \cos\theta)(r^2 - r_i^2)(r^2 - r_o^2)\sin t \tag{A3}$$

if we choose

$$f_0 = \frac{\partial H_0}{\partial t} - \nabla^2 H_0.$$

Let H^{n+1} and H^n denote the values of H at the time steps $t = t_{n+1}$ and $t = t_n$ respectively. Equation (A1) can be written as

$$\frac{H^{n+1} - H^n}{\Delta t} - \frac{1}{r^2}\frac{\partial}{\partial r}\left[r^2 \frac{\partial}{\partial r}(H^{n+1} - H^n) \right] = \nabla^2 H^n + f^n, \tag{A4}$$

where the radial direction is treated implicitly while the azimuthal and latitudinal directions are treated explicitly. In this way, the resulting matrix is tridiagonal and can be effectively

TABLE III. The accuracy of the numerical solutions at different spatial resolution, where n_ϕ, n_θ, and n_r are the grid numbers in the azimuthal, latitudinal, and radial directions and Δt denotes the time step in numerical simulations.

$(n_\varphi \times n_\theta \times n_r)$	Δt	Err
$40\times36\times10$	5×10^{-5}	8.03×10^{-4}
$40\times36\times20$	5×10^{-5}	2.78×10^{-6}
$40\times36\times25$	5×10^{-5}	1.66×10^{-6}
$40\times36\times27$	5×10^{-5}	1.41×10^{-6}
$40\times36\times30$	5×10^{-5}	1.13×10^{-6}
$40\times36\times35$	5×10^{-5}	8.61×10^{-7}

solved on a parallel computer by a domain decomposition method (see Fig. 2).

The fully numerical solution for Eq. (A1), i.e., $H_{\text{numerical}}$, can be then compared with the corresponding exact solution. The accuracy of the numerical solution is measured by

$$\text{Err} = \frac{1}{V}\int_V |H_{\text{exact}} - H_{\text{numerical}}|^2 dV,$$

where V denotes the volume of the spherical shell. In Table III, we show several numerical solutions calculated using different spatial resolutions for $r_i/r_o=0.5$. It can be seen that the exact solution is well approximated when $n_\varphi=40$, $n_\theta=36$ and $n_r=20$. In our actual numerical simulation for nonlinear convection in spherical shells, the spatial resolution is checked by varying values of n_ϕ, n_θ, and n_r. The spatial resolution used in our nonlinear simulation is typically $n_\phi=O(100)$, $n_\theta=(100)$, and $n_r=40$.

[1] R. E. Grimm and H. Y. McSween, "Water and the thermal evolution of carbonaceous chondrite parent bodies," Icarus **82**, 244 (1998).
[2] E. D. Young, K. Zhang, and G. Schubert, "Conditions for pore water convection within carbonaceous chondrite parent bodies: implication for planetesimal size and heat production," Earth Planet. Sci. Lett. **213**, 249 (2003).
[3] K. Zhang, X. Liao, and G. Schubert, "Pore water convection within carbonaceous chondrite parent bodies: Temperature-dependent viscosity and flow structure," Phys. Fluids **17**, 086602 (2005).
[4] R. E. Young, "Finite-amplitude thermal convection in a spherical shell," J. Fluid Mech. **63**, 695 (1974).
[5] F. H. Busse, "Patterns of convection in spherical shells," J. Fluid Mech. **72**, 67 (1975).
[6] P. C. Matthews, "Pattern formation on a sphere," Phys. Rev. E **67**, 036206 (2003).
[7] P. Chossat, "Bifurcation and stability of convective flows in a rotating or not rotating spherical shell," SIAM J. Appl. Math. **37**, 627 (1979).
[8] G. Schubert, "Subsolidus convection in the mantle of terrestrial planets," Annu. Rev. Fluid Mech. **7**, 289 (1979).
[9] G. Schubert and A. Zebib, "Thermal convection of an internally heated infinite Prandtl number fluid in a spherical shell," Geophys. Astrophys. Fluid Dyn. **15**, 65 (1980).
[10] G. A. Glatzmaier, "Numerical simulations of mantle convection: time-dependent, three-dimensional, compressible, spherical shell," Geophys. Astrophys. Fluid Dyn. **43**, 223 (1988).
[11] K. Zhang and F. H. Busse, "Convection in spherical fluid shell with an outer crust of variable thickness," Phys. Earth Planet. Inter. **104**, 283 (1997).
[12] S. Zhong, M. T. Zuber, L. N. Moresi, and M. Gurnis, "Role of temperature dependent viscosity and surface plates in spherical shell models of mantle convection," J. Geophys. Res. **105**, 11063, DOI: 10.1029/2000JB900003 (2000).
[13] D. A. Yuen, S. Balachandar, and U. Hansen, "Modelling mantle convection: A significant challenge in geophysical fluid dynamics," in *Geophysical and Astrophysical Convection*, edited by P. A. Fox and R. M. Kerr (Gordon and Breach, New York, 2000), pp. 257.
[14] K. Stemmer, H. Harder, and U. Hansen, "A new method to simulate convection with strongly temperature and pressure-dependent viscosity in a spherical shell: Application to the Earth's mantle," Phys. Earth Planet. Inter. **157**, 223 (2006).
[15] K. H. Chan, L. Li, and X. Liao, "Modelling the core convection using finite element and finite difference methods," Phys. Earth Planet. Inter. **157**, 124 (2006).
[16] S. Chandrasekhar, *Hydrodynamic and Hydromagnetic Stability* (Clarendon, Oxford, 1961).
[17] P. Olson and G. M. Corcos, "A boundary layer model for mantle convection with surface plates," Geophys. J. R. Astron. Soc. **62**, 195 (1980)
[18] U. Hansen and A. Ebel, "Experiments with a numerical model related to mantle convection: Boundary layer behaviour of small and large-scale flows," Phys. Earth Planet. Inter. **36**, 374 (1984).
[19] G. Schubert, J. D. Anderson, B. J. Travis, and J. Palguta, "Enceladus: Present internal structure and differentiation by early and long-term radiogenic heating," Icarus **188**, 345 (2007).